

Connecting the one-band and three-band Hubbard models of cuprates via spectroscopy and scattering experiments

K. Sheshadri,¹ D. Malterre,² A. Fujimori,^{3,4,5} and A. Chainani⁵

¹226, Bagalur, Bangalore North, Karnataka State, India 562149

²Institut Jean Lamour, Université de Lorraine, UMR 7198 CNRS, BP70239, 54506 Vandoeuvre lés Nancy, France

³Department of Physics, The University of Tokyo,

7-3-1 Hongo, Bunkyo-ku, Tokyo 113-0033, Japan

⁴Center for Quantum Science and Technology and Department of Physics,
National Tsing Hua University, Hsinchu 30013, Taiwan

⁵Condensed Matter Physics Group, National Synchrotron Radiation Research Center, Hsinchu 30076, Taiwan

(Dated: January 10, 2023)

The one-band and three-band Hubbard models which describe the electronic structure of cuprates indicate very different values of effective electronic parameters, such as the on-site Coulomb energy and the hybridization strength. In contrast, a comparison of electronic parameters of several cuprates with corresponding values from spectroscopy and scattering experiments indicates similar values in the three-band model and cluster model calculations used to simulate experimental results. The Heisenberg exchange coupling J obtained by a downfolding method in terms of the three band parameters is used to carry out an optimization analysis consistent with J from neutron scattering experiments for a series of cuprates. In addition, the effective one-band parameters \tilde{U} and \tilde{t} are described using the three band parameters, thus revealing the hidden equivalence of the one-band and three-band models. The ground-state singlet weights obtained from an exact diagonalization elucidates the role of Zhang-Rice singlets in the equivalence. The results provide a consistent method to connect electronic parameters obtained from spectroscopy and the three-band model with values of J obtained from scattering experiments, band dispersion measurements and the effective one-band Hubbard model.

I. INTRODUCTION

The mechanism of high-temperature superconductivity exhibited by the copper-oxide families of layered compounds remains one of the most intriguing and challenging topics in condensed matter physics¹, nearly 36 years after its discovery². The discovery of copper-oxide based superconductivity led to unprecedented theoretical and experimental efforts to understand the phenomenon. While there have been innumerable models put forth to understand the mechanism of high-temperature superconductivity, it still remains an open problem. On the other hand, nearly all the models agree that superconductivity in the copper-oxide based materials is intimately associated with quasi two-dimensionality (2D) and strong electron-electron correlations¹. This is based on the fact that the CuO₂ planes are the main source of the electronic states which undergo the superconducting transition. At a very broad level, the possible mechanisms discussed in the literature span over various models including the effective one-band Hubbard model^{3,4}, resonating valence bond theory⁵, the three-band Hubbard model^{6,7}, the t-J model⁸, spin-fluctuation driven pairing⁹, marginal Fermi liquid¹⁰, pair density wave model¹¹, electron-phonon coupling-induced pairing which go beyond the BCS model¹², and so on.

The simplest parent compound La₂CuO₄ is a good antiferromagnetic insulator and upon hole-doping, undergoes a transition to a dome shaped superconducting phase with an optimal $T_c \sim 38$ K². While the long-range order is lost, La_{2-x}Sr_xCuO₄, as well as several other cop-

per oxide superconductors, continue to exhibit antiferromagnetic correlations in the form of resonant modes and paramagnons in the superconducting phase¹³⁻¹⁵. In fact, along with superconductivity, all the families of copper oxide superconductors also show spin- and charge-ordering phenomena¹⁶⁻²⁵ which suggest a complex co-existence of electron-phonon coupling, spin fluctuations and electron-electron correlation effects^{26,27}.

The basic starting point to understand cuprate properties is often considered to be the 2D Hubbard model involving strong electron-electron correlations with strong Cu-O hybridization leading to the Zhang-Rice singlet (ZRS) ground state⁴. It is well-known and well-accepted that the parent copper-oxide materials are best described as charge-transfer insulators in the Zaanen-Sawatzky-Allen scheme²⁸, with the copper on-site Coulomb energy $U_d \gg \Delta$, the charge-transfer energy, and the lowest energy excitations involve the strongly hybridized Cu-3d and O-2p ZRS states. Further, hole doping in the parent compound results in oxygen hole carriers retaining the ZRS character of the lowest energy excitations²⁹⁻³¹.

A very important issue involves how to quantify electron-electron correlations in any transition metal compound, in general, and the cuprates, in particular^{32,33}. Depending on the theoretical model, the values of electron-electron correlation strength can be very different for the same material. A comparison of the effective one band Hubbard model^{3,4} consisting of the single antibonding band made up of the Cu $d_{x^2-y^2}$ and O p_x, p_y orbitals, and the effective three band Hubbard model^{6,7} which describes the cuprate electronic structure

in terms of the Cu-O bonding, non-bonding and anti-bonding bands show significantly different values of on-site Coulomb energy in the Cu d states. In the following, in order to distinguish the one band and three band parameters, we use the notation U_d/U_p and t_{pd} for the Cu/O on-site Coulomb energies and hopping in the three band model, while \tilde{U} and \tilde{t} are used for the one-band Hubbard model, respectively. Thus, for example, while early studies of the three band model estimated $U_d \sim 7\text{-}10$ eV and $U_p \sim 3\text{-}6$ eV³⁴⁻³⁶, typical values of $\tilde{U} \sim 3\text{-}4$ eV are known for the effective one-band model^{37,38}.

It is noted that while several theoretical studies have included the oxygen on-site Coulomb energy U_p , there are also some studies which have neglected U_p . For example, early theory⁷, and cluster model calculations of core-level photoemission and optical absorption³⁹⁻⁴² could explain experimental results fairly well but in the absence of U_p . In a study using the coherent potential approximation, an effective one-band model was obtained from the three band model including the inter-site Coulomb energy U_{pd} treated in the Hartree-Fock approximation, but with $U_p = 0$ ^{43,44}. The authors showed that the effective \tilde{U} increased on increasing U_{pd} , and they could obtain a metal-insulator phase diagram as a function of U_d and Δ . In a three-band Hubbard model using the constrained-path Monte Carlo method, the binding energy of a pair of holes and the symmetry of superconducting pairing correlation functions was investigated, but in the absence of U_p ⁴⁵. Cluster perturbation theory applied to calculate spectral functions of cuprates also did not include U_p , but could show spin-charge separation in the 1D Hubbard model, as well as momentum-dependent spectral-weight in the 2D Hubbard model⁴⁶. Cluster dynamical mean field theory approximation was used to investigate the three-band Hubbard model in the absence of U_p and showed that the cuprates can be described as magnetically correlated Mott insulators⁴⁷. More recently, quantum Monte Carlo calculations demonstrated dynamical stripe correlations in the three-band Hubbard model without U_p , and also explained experimental observations such as the hourglass magnetic dispersion⁴⁸. The three-band Hubbard model using the auxiliary-field quantum Monte Carlo method, but without U_p , was used to show the importance of Δ and a quantum phase transition from an antiferromagnetic insulator to paramagnetic metal for $\Delta < 3$ eV⁴⁹.

However, electron spectroscopy studies in conjunction with cluster model calculations or using the Cini-Sawatzky method^{50,51} have estimated $U_d \sim 6 - 8$ eV^{39,40,52} and $U_p \sim 5 - 6$ eV⁵³⁻⁵⁵. Thus, U_d and U_p are comparable and needed for describing the electronic states derived from Cu-O planes, particularly in the charge transfer limit, as U_p gets close to or larger than Δ .

Further, an *ab initio* method with dynamical screening³⁷ applied to the one-band model for La_2CuO_4 estimated a static $\tilde{U}(w=0) \sim 3.65$ eV, while for the three-band model, it gave $U_d(w=0) \sim 7.0$ eV and $U_p(w=0) \sim 4.64$ eV. Another very recent multi-scale *ab initio* method³⁸ applied to the one band model for La_2CuO_4 estimated $\tilde{U} \sim 5.0$ eV, while for the three-band model it estimated $U_d \sim 9.6$ eV and $U_p \sim 6.1$ eV. It is noted that the models have also estimated the inter-site Coulomb energies, as well as the nearest and next-nearest-neighbour hopping (t and t') which also show differences depending on the method³⁴⁻³⁸.

Very interestingly, Hubbard-type cluster models employing $d_{x^2-y^2}$, p_x and p_y levels have been extensively used for calculating spectra in high energy spectroscopies like core-level photoemission (PES) and x-ray absorption (XAS), resonant inelastic x-ray scattering (RIXS) structure factors, etc. and the obtained electronic parameters^{53-55,62-77} are quite close to the theoretical estimates from the effective three-band model^{34-36,38,78} (see Tables I and II). It is noted that the effective three-band model parameters were also used to calculate the dynamical spin structure factor of Bi2201 measured by RIXS⁷⁷. On the other hand, analysis of neutron scattering measurements of magnon dispersions⁵⁹ and angle-resolved photoemission spectroscopy (ARPES) band dispersions^{60,61} of parent cuprates have employed the extended one-band Hubbard model or the extended $t - J$ model to study the nearest neighbor exchange interaction and correlation effects, and they obtained electronic parameter values close to the values obtained from the effective one-band theoretical models.

For example, it was shown that neutron scattering of La_2CuO_4 provided a dominant nearest neighbor (NN) hopping $t = 0.33$ eV and an effective $U/t = 8.8$ with $U = 2.9$ eV, but also showed that in addition to the NN exchange $J = 138$ meV, it was important to include ring exchange $J_c = 38$ meV, while $J' = J'' = 2$ meV were small⁵⁹. Similarly, for $\text{Sr}_2\text{CuO}_2\text{Cl}_2$, the $t - t' - t'' - J$ model showed $t = 0.35$ eV, while $t' = 0.12$ eV, and $t'' = 0.08$ eV, and with a $J = 0.14$ eV⁶¹, it implied an effective $\tilde{U}/t = 10$ with $\tilde{U} = 3.5$ eV. Thus, in these cases, the results suggest that the NN hopping t and U can be considered to be the \tilde{t} and \tilde{U} of the one-band model. For CuO , a recent study showed that a linear spin-wave model for a Heisenberg antiferromagnet provided a good description of the neutron scattering results⁷⁹. The relevant exchange constants could be accurately determined and showed that the dominant exchange interaction $J = 91$ meV, which coupled antiferromagnetically along the $[10\bar{1}]$ chain direction, while the nearest neighbor inter-chain interactions were very weak ($J_{ac} = 3.9$ meV and $J_b = 0.39$ meV) and coupled ferromagnetically⁷⁹.

TABLE I: Electronic parameters (U_d , t_{pd} , Δ , U_p) for cuprates from the three-band Hubbard model (Theory) and from cluster model calculations (Spectroscopy and RIXS). The table also shows two optimized parameter sets (Δ_1 and U_{p1}) and (t_{pd2} and Δ_2) with their cost functions f_1 and f_2 , respectively. J is the nearest-neighbor Heisenberg exchange deduced from scattering experiments. See text for details.

Compound (ref. no)	U_d ± 0.5 eV	t_{pd} ± 0.2 eV	Δ ± 1.0 eV	U_p ± 0.5 eV	Optimization-1			J (ref.no) ± 5 meV	Optimization-2		
					Δ_1 eV	U_{p1} eV	f_1		t_{pd2} eV	Δ_2 eV	f_2
Theory											
La ₂ CuO ₄ (34)	9.4	1.5	3.5	4.7	5.7	4.9	5.09	140 (59)	1.1	3.7	0.96
La ₂ CuO ₄ (35)	10.5	1.3	3.6	4.0	4.5	4.1	1.01	140 (59)	1.2	3.7	0.4
La ₂ CuO ₄ (36)	8.8	1.3	3.5	6.0	4.5	6.1	0.98	140 (59)	1.2	3.7	0.38
La ₂ CuO ₄ (38)	9.61	1.37	3.7	6.1	4.6	6.2	0.79	140 (59)	1.2	3.9	0.36
Hg1201(38)	8.84	1.26	2.42	5.3	4.4	5.4	3.78	135 (76)	0.9	2.6	0.75
Bi2212(78)	8.5	1.13	3.2	4.1	3.5	4.1	0.06	161 (76)	1.1	3.5	0.06
Spectroscopy											
CuO(54,65)	7.7	1.55	2.5	5	7.6	5.4	25.9	91 (79*)	0.8	2.6	1.72
Sr ₂ CuO ₃ (62,63)	8.8	1.45	2.5	4.4	4.4	4.6	3.62	241 (71)	1.1	2.8	0.96
Sr ₂ CuO ₂ Cl ₂ (64)	8.8	1.5	3.5	4.4	6.0	4.6	6.45	130(60,61)	1.1	3.7	1.04
La ₂ CuO ₄ (65,66)	7.0	1.5	3.5	6.0	6.0	6.2	6.49	140 (59)	1.13	3.7	1.0
Nd ₂ CuO ₄ (67)	8.0	1.1	3.0	4.1	3.6	4.1	0.41	133 (72)	1.0	3.2	0.21
Pr ₂ CuO ₄ (67)	8.0	1.1	3.0	4.1	3.8	4.2	0.62	121 (72)	1.0	3.2	0.26
YBCO(53,55)	7.0	1.2	1.5	5.0	4.4	5.2	8.2	125 (73)	0.7	1.7	0.99
Bi2212(70)	7.7	1.5	3.5	6.0	5.6	6.1	4.3	161 (76)	1.2	3.7	0.88
RIXS											
Bi2201(77)	10.2	1.35	3.9	5.9	4.5	5.9	0.34	153(76,77)	1.3	4.1	0.22

(*For CuO, the dominant exchange interaction J which couples antiferromagnetically is the one along the $[10\bar{1}]$ chain direction and considered here, while the nearest neighbor spins exhibit a weak ferromagnetic coupling (ref. 79).)

TABLE II: Renormalized electronic parameters \tilde{U} and \tilde{t} for cuprates in the one-band Hubbard model along with the ground state singlet weights c_{21} (between the two Cu sites) and c_{13} (between the Cu and O site). Optimization-1 uses (U_d , t_{pd} , Δ_1 , U_{p1}) and Optimization-2 uses (U_d , t_{pd2} , Δ_2 , U_p) from Table I to obtain corresponding \tilde{U} and \tilde{t} .

Compound	Optimization-1			J meV	Optimization-2			c_{21}	c_{13}
	\tilde{U} eV	\tilde{t} eV	\tilde{U}/\tilde{t}		\tilde{U} eV	\tilde{t} eV	\tilde{U}/\tilde{t}		
Theory									
La ₂ CuO ₄ (34)	4.38	0.39	11.18	140	3.68	0.36	10.26	0.65	0.2
La ₂ CuO ₄ (35)	4.03	0.37	10.73	140	3.7	0.36	10.28	0.65	0.2
La ₂ CuO ₄ (36)	4.05	0.38	10.76	140	3.81	0.37	10.42	0.64	0.2
La ₂ CuO ₄ (38)	4.27	0.41	10.43	140	4.05	0.4	10.16	0.64	0.2
Hg1201(38)	3.93	0.36	10.79	135	3.3	0.33	9.89	0.63	0.21
Bi2212(78)	3.35	0.37	9.13	161	3.34	0.37	9.11	0.64	0.2
Spectroscopy									
CuO(54,65)	4.39	0.32	13.87	91	3.09	0.27	11.62	0.64	0.2
Sr ₂ CuO ₃ (62,63)	3.79	0.48	7.94	241	3.17	0.44	7.25	0.62	0.23
Sr ₂ CuO ₂ Cl ₂ (64)	4.28	0.37	11.47	130	3.53	0.34	10.42	0.65	0.19
La ₂ CuO ₄ (65,66)	3.96	0.37	10.64	140	3.42	0.34	9.89	0.64	0.2
Nd ₂ CuO ₄ (67)	3.33	0.33	10.01	133	3.17	0.32	9.75	0.64	0.2
Pr ₂ CuO ₄ (67)	3.38	0.32	10.58	121	3.16	0.31	10.23	0.64	0.2
YBCO(53,55)	3.49	0.33	10.56	125	2.61	0.29	9.14	0.62	0.23
Bi2212(70)	4.07	0.4	10.05	161	3.59	0.38	9.44	0.64	0.2
RIXS									
Bi2201(77)	4.31	0.41	10.61	153	4.18	0.4	10.45	0.65	0.2

Given the differences in electronic parameters between the theoretical one-band versus the three-band models, and the corresponding experimental high-energy spec-

troscopies versus the low-energy magnon and band dispersion measurements, we felt it important to address a possible connection between them. In this study, we

TABLE III: Examples of one-band model electronic parameters estimated independently from magnon dispersion in neutron scattering, band dispersion in ARPES, and from *ab initio* theory.

Compound (ref. no)	\tilde{U} eV	\tilde{t} eV	\tilde{U}/\tilde{t}	Method
La ₂ CuO ₄ (57)	2.9	0.33	8.8	Neutron scattering
Sr ₂ CuO ₂ Cl ₂ (58,59)	3.5	0.35	10.0	ARPES
La ₂ CuO ₄ (38)	5.0	0.48	10.4	<i>ab initio</i> theory
Hg1201 (38)	4.4	0.46	9.5	<i>ab initio</i> theory

have found an equivalence by using the nearest neighbor Heisenberg exchange interaction J obtained from neutron scattering and RIXS experiments^{59,71–77,79} as a bridge to connect electronic parameters known from experiment (high-energy spectroscopy, RIXS, neutron scattering) and theoretical estimates obtained from the one-band and three-band Hubbard models. The results show that the three-band Hubbard model parameters can be used to describe J in terms of the well-known one-band Hubbard model form of $J = 4\tilde{t}^2/\tilde{U}$ with renormalized parameters \tilde{U} and \tilde{t} .

We now summarize our main results. We calculate J , the strength of the Heisenberg coupling between Cu moments in a Cu₂O cluster, using the downfolding method discussed by Koch³³. For several compounds neutron scattering data for J and spectroscopic data for U_d , U_p , Δ and t_{pd} are available. Directly using the spectroscopic parameter values in the downfolding expression for J leads to deviations from the experimental J values. We therefore use two estimation procedures, referred to as Optimization-1 and Optimization-2 in the following, to modify a subset (different in the two procedures) of the spectroscopic data, so that there is a good agreement with experimental J values using the procedure described in Sec. II. We identify effective parameters \tilde{t} and \tilde{U} so that the downfolding expression for J becomes equal to $4\tilde{t}^2/\tilde{U}$. The estimated values of \tilde{t} and \tilde{U} are found to be consistently smaller than t_{pd} and U_d in all cases, but lead to a larger \tilde{U}/\tilde{t} in the one-band case compared to the U_d/t_{pd} of the three-band case, in good agreement with theoretical estimates reported in the literature. The results indicate that stronger effective correlations, arising from a combination of U_d , U_p , Δ and t_{pd} are hidden in the effective one-band Hubbard model. The study provides a consistent method to connect electronic parameters obtained from spectroscopy and the three-band model with effective parameters obtained from neutron scattering, ARPES measurements and the one-band Hubbard model.

II. CALCULATIONS

We consider a Cu₂O cluster with site labels $i = 1, 2$ (for Cu(1) and Cu(2) atoms) and $i = 3$ (for the O atom). The cluster hamiltonian is

$$\hat{H} = \frac{\Delta}{2}(n_3 - n_1 - n_2) - t_{pd} \sum_{i\sigma} (d_{i\sigma}^\dagger p_\sigma + h.c.) + U_d(n_{1\uparrow}n_{1\downarrow} + n_{2\uparrow}n_{2\downarrow}) + U_p n_{3\uparrow}n_{3\downarrow}, \quad (1)$$

where $n_{i\sigma}^d = d_{i\sigma}^\dagger d_{i\sigma}$ ($i = 1, 2$), $n_{3\sigma} = p_\sigma^\dagger p_\sigma$ and $n_i = n_{i\uparrow} + n_{i\downarrow}$. Here, $d_{i\sigma}^\dagger$ creates a hole with a z component of spin $\sigma = \pm 1/2$ in the Cu d orbital at site i ($= 1, 2$), and p_σ^\dagger creates a hole with a z component of spin $\sigma = \pm 1/2$ in the O p orbital at the site located in between the two Cu sites. Δ is the charge-transfer energy; the parameters U_p and U_d are on-site Coulomb energies at the O and Cu sites, respectively; and finally t_{pd} is the strength of hopping between neighboring O and Cu sites.

In this work, we consider a filling fraction corresponding to undoped cuprates, in which the outermost p orbital on the O site is filled with two electrons (i.e. empty in the hole picture), and the outermost d orbital on the Cu site has one electron (i.e. one hole), in the absence of hopping. For our cluster with three atoms, this corresponds to a total occupancy of four electrons, or two holes. The two holes can be selected in three ways: both with $\sigma = -1/2$ (the ferromagnetic down case), both with $\sigma = 1/2$ (the ferromagnetic up case), and finally, one hole with $\sigma = 1/2$ and another with $\sigma = -1/2$ (the antiferromagnetic case).

We will consider only the antiferromagnetic case henceforth. In this case, there are 9 basis states $|i, j\rangle$, $i, j = 1, 2, 3$. In state $|i, j\rangle$, i and j are the Cu ($i, j = 1, 2$) or O ($i, j = 3$) sites with up and down holes, respectively. In the basis $\{|1, 2\rangle, |2, 1\rangle, |1, 3\rangle, |3, 1\rangle, |2, 3\rangle, |3, 2\rangle, |1, 1\rangle, |2, 2\rangle, |3, 3\rangle\}$, the hamiltonian (1) becomes a 9×9 matrix

$$H = \begin{bmatrix} H_{00} & H_{01} & H_{02} \\ H_{10} & H_{11} & H_{12} \\ H_{20} & H_{21} & H_{22} \end{bmatrix}, \quad (2)$$

in which the blocks are

$$\begin{aligned}
H_{00} &= -\Delta \begin{bmatrix} 1 & 0 \\ 0 & 1 \end{bmatrix}, \quad H_{01} = \begin{bmatrix} t_{pd} & 0 & 0 & -t_{pd} \\ 0 & t_{pd} & -t_{pd} & 0 \end{bmatrix}, \\
H_{02} &= O_{2 \times 3}, \quad H_{11} = O_{4 \times 4}, \quad H_{12} = \begin{bmatrix} t_{pd} & 0 & t_{pd} \\ -t_{pd} & 0 & -t_{pd} \\ 0 & t_{pd} & t_{pd} \\ 0 & -t_{pd} & -t_{pd} \end{bmatrix}, \\
\text{and } H_{22} &= \begin{bmatrix} U_d - \Delta & 0 & 0 \\ 0 & U_d - \Delta & 0 \\ 0 & 0 & U_p + \Delta \end{bmatrix}. \quad (3)
\end{aligned}$$

In the above, $O_{m \times n}$ denotes an $m \times n$ matrix of zeros. We calculate the Heisenberg antiferromagnetic coupling J between the Cu(1) and Cu(2) spins based on the downfolding fourth-order perturbation method described in Koch³³ and Zurek⁸⁰. Accordingly, the effective hamiltonian is

$$\begin{aligned}
\tilde{H} &= H_{00} + H_{01}(\epsilon - (H_{11} + H_{12}(\epsilon - H_{22})^{-1}H_{21})^{-1})^{-1} \\
&\approx H_{00} + H_{01}(\epsilon - H_{11})^{-1}H_{10} + \\
&\quad H_{01}(\epsilon - H_{11})^{-1}H_{12}(\epsilon - H_{22})^{-1}H_{21}(\epsilon - H_{11})^{-1}H_{10}
\end{aligned} \quad (4)$$

where we have used the approximation $(A + B)^{-1} \approx A^{-1}(1 - BA^{-1})$. We now take $\epsilon = -\Delta$ and perform the matrix products above. The result is

$$\tilde{H} \approx -\frac{2t_{pd}^2}{\Delta} \begin{bmatrix} 1 & 0 \\ 0 & 1 \end{bmatrix} - \frac{J}{2} \begin{bmatrix} 1 & -1 \\ -1 & 1 \end{bmatrix} \quad (5)$$

where the Heisenberg coupling is

$$J = 4 \frac{t_{pd}^4}{\Delta^2} \left[\frac{1}{U_d} + \frac{1}{\Delta + U_p/2} \right]. \quad (6)$$

The result we have obtained for J using the downfolding approximation is the same as that reported in earlier studies^{32,56,57} using a fourth-order perturbation theory. If we now define \tilde{t} and \tilde{U} using

$$\tilde{t} = \frac{t_{pd}^2}{\Delta}, \quad \frac{1}{\tilde{U}} = \frac{1}{U_d} + \frac{1}{\Delta + U_p/2} \quad (7)$$

then $J = 4\tilde{t}^2/\tilde{U}$. This is the expression for J we would get if we used a one-band Hubbard model with a hopping strength \tilde{t} and an on-site repulsion $\tilde{U} \gg \tilde{t}$, using second-order perturbation theory. In this sense, we consider \tilde{U} and \tilde{t} as the parameters of an effective one-band Hodel model corresponding to the model in (1).

We find that using the spectroscopic values on the right-hand side and the experimental J values on the left-hand side of equation (6) does not satisfy the equation with sufficient accuracy. We therefore modify, in an optimal manner described below, a subset of the spectroscopic parameter values so that the agreement is good.

We now describe two such simple optimization procedures. We define the parameter $R = \tilde{U}/\tilde{t}$ to obtain the

parametric forms $\tilde{t} = RJ/4$, $\tilde{U} = R^2J/4$ for the effective parameters. These are the expressions that we use below for \tilde{t} , \tilde{U} .

In the Optimization-1 procedure, we modify (Δ, U_p) . We solve the relations (7) to obtain $\Delta_1(R) = t_{pd}^2/\tilde{t}$ and $U_{p1}(R)/2 = U_d\tilde{U}/(U_d - \tilde{U}) - \Delta_1(R)$. We then minimize a cost function $f_1(R) = (\Delta_1(R) - \Delta)^2 + (U_{p1}(R) - U_p)^2$ with respect to R to obtain the minimum R^* , using the spectroscopic values for U_d , U_p , Δ , t_{pd} and neutron scattering values for J . This estimates $\Delta_1(R^*)$, $U_{p1}(R^*)$, $\tilde{U}(R^*)$, and $\tilde{t}(R^*)$.

In the Optimization-2 procedure, we modify (Δ, t_{pd}) . We solve the relations (7) to obtain $t_{pd2}(R)^2 = \Delta_2(R)\tilde{t}$ and $\Delta_2(R) = U_d\tilde{U}/(U_d - \tilde{U}) - U_p/2$. We then minimize a cost function $f_2(R) = (\Delta_2(R) - \Delta)^2 + |(t_{pd2}(R)^2 - t_{pd}^2)|$ with respect to R to obtain the minimum R^* , using the spectroscopic values for U_d , U_p , Δ , t_{pd} and neutron scattering values for J . This estimates $\Delta_2(R^*)$, $t_{pd2}(R^*)$, $\tilde{U}(R^*)$, and $\tilde{t}(R^*)$.

III. RESULTS AND DISCUSSION

The results are summarized in Table I and Table II for a variety of CuO-based materials. Table I presents our estimates of the theoretical and spectroscopic three-band model parameters, while Table II presents our estimates of effective one-band parameters. Both tables contain results of the two optimization procedures that we discussed above.

In Table I, the columns 5-7 present results of Optimization-1 procedure: these are values of Δ_1, U_{p1} and f_1 ; the columns 9-11 present results of Optimization-2 procedure: these are values of t_{pd2}, Δ_2 and f_2 . We can see from the cost function values that Optimization-2 is better than Optimization-1; this is also reflected in the greater closeness of (t_{pd2}, Δ_2) estimates to measured values than that of (Δ_1, U_{p1}) estimates to measured values. Considering that J depends on t_{pd}^4 in equation (6), it can be seen that a smaller spread in t_{pd} across compounds provides a better description of parameter values; further since Δ and t_{pd} are intimately related through the first relation in equation (7), it makes sense to optimize with respect to these two parameters as is done in Optimization-2. This has the result of reducing the spread in estimated t_{pd2} values compared with reported spectroscopic t_{pd} values. This also improves the estimates of Δ compared to Δ_1 in Optimization-1. For these reasons, we can understand that Optimization-2 is better than not only Optimization-1, but also other possible optimization choices, namely (Δ, U_d) , (t_{pd}, U_p) and (t_{pd}, U_d) . We therefore do not present the results of these latter procedures.

Since $R = \tilde{U}/\tilde{t} \sim 10$ in most cases (see columns 4 and 8 in Table II), we can see that it makes sense to treat \tilde{U} , \tilde{t} as effective one-band parameters, as is known from earlier work (Table III). We observe that $R \sim 10$ not

only in cases where spectroscopic three-band parameter values are reported, but also for theoretical as well as RIXS three-band parameter values (see Table II).

Secondly, \tilde{U} is roughly half of U_d in almost all cases. This shows that the effective model is not a simple Cu d -band model, but possibly a more hybrid one involving Cu- d and O- (p_x, p_y) orbitals. To understand this better, we have looked at the nature of the ground state obtained by exactly diagonalizing the cluster hamiltonian (1) for each compound in Table I using our Optimization-2 estimates of the three-band parameters. The ground state we obtain, $|G\rangle = \sum_{ij} c_{ij} |i, j\rangle$, always has the property $c_{12} = -c_{21}, c_{13} = -c_{31} = c_{23} = -c_{32}, c_{11} = c_{22}$ by symmetry, which shows that it is a singlet of Cu and O orbitals. We can thus completely characterize the ground state with the two distinct singlet weights c_{21} and c_{13} and the two distinct hole double-occupancy weights c_{11} and c_{33} . Since our focus is primarily on the singlet nature of $|G\rangle$, we present c_{21} and c_{13} in Table II (see columns 9 and 10). The singlet weights of the Cu-Cu and Cu-O sectors confirm that the ground state is a ZRS. The effective interaction \tilde{U} is thus not between purely Cu- d holes, but represents the hybrid ZR singlets, and is therefore significantly smaller than U_d . However, it must also be noted from Table I and Table II that $\tilde{U}/\tilde{t} \simeq 10$, satisfying the strong correlation condition in the effective one-band model. In Table III, we list a few examples of one-band model electronic parameters estimated independently, from magnon dispersion in neutron scattering, band dispersion in ARPES and from *ab initio* theory. It is clear that the values of \tilde{U}/\tilde{t} in all the cases are close to the values in Table II and validates our analysis.

Finally, in Fig. 1(a-d) we present plots of various $|c_{ij}|^2$ as a function of t_{pd} , for $U_p = 1, 3$ and 5 eV; we have fixed the values $U_d=8$ eV and $\Delta = 3.3$ eV (=average Δ of values obtained by optimization 2 shown in Table I) in these plots. Fig. 1(a) shows that the pure Cu(1)-Cu(2) singlet weight $2|c_{12}|^2 \sim 1$ obtained for $t_{pd} = 0$ systematically reduces in weight on increasing t . Simultaneously, the total Cu(1)-O(3) singlet weight $4|c_{13}|^2$ increases systematically on increasing t_{pd} , indicating the role of Cu-O hybridization in forming the ZRS state for the cuprates. Thus, the O- p orbital plays an increasingly important role on increasing t_{pd} to ~ 1 eV, typical of the cuprates. Further, the on-site double occupancy weights $|c_{ii}|^2$, $i = 1-3$, are quite small (Fig. 1(c,d)). However, on increasing U_p from 1 to 5 eV, while there is hardly any change in the total double occupancy weight $2|c_{11}|^2$ on the Cu sites, the double occupancy weight $|c_{33}|^2$ on the O site gets suppressed to nearly half its value for $t_{pd} > 1$ eV. This behavior of the O site double occupancy is closely related to the reduction of J by U_p according to Eq. (6). Thus, U_p plays an important role in tuning the value of J , which is considered to be one of the most important parameters to achieve high-temperature superconductivity exhibited by the family of cuprates^{1,59,71-77,81-84}.

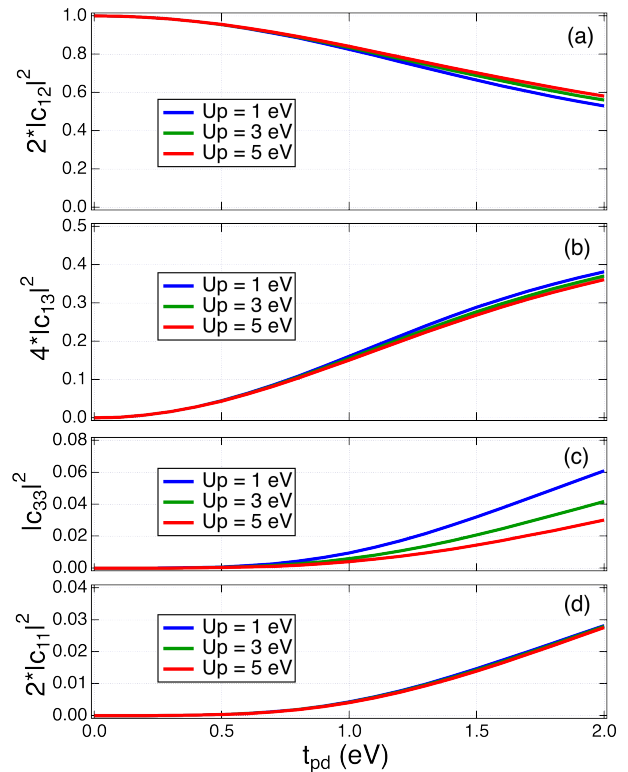


FIG. 1: (a-d) Plots of various calculated total weights $|c_{ij}|^2$ as a function of t_{pd} , for $U_d=8$ eV, $\Delta = 3.3$ eV and $U_p= 1, 3$ and 5 eV. (a) shows the total Cu(1)-Cu(2) singlet weight $2|c_{12}|^2$. (b) shows the total Cu(1)-O(3) singlet weight $4|c_{13}|^2$. (c) and (d) show the on-site double occupancy weights $|c_{11}|^2$ (total for the Cu(1) and Cu(2) sites) and $|c_{33}|^2$ for the O(3) site.

IV. CONCLUDING REMARKS

In this work, we have presented a data analysis of spectroscopic parameters and neutron-scattering parameters for a variety of cuprates based on a theoretical relationship between the parameters of a three-band model and an effective one-band Heisenberg antiferromagnetic coupling, using a cluster-model calculation. We have also performed an exact diagonalization of the cluster hamiltonian to understand the nature of the ground state.

Our analysis shows $\tilde{U} < U_d$ always. In addition to agreeing with estimates of \tilde{U} from the one-band model applied to neutron scattering or ARPES experiments, this inequality is a direct consequence of equation (7).

U_p is significant in magnitude, both in measurements and in our estimates, and is not small compared to U_d . While U_p has been neglected in some studies on cuprates, we believe it is as important as U_d . Further, the second relation in equation (7) shows that the effective interaction \tilde{U} is enhanced by U_p and Δ .

The ground-state singlet weights from our exact diagonalization show the importance of O moments and ZRS in the effective description. We also observe that

the singlet weights change very little across the family of compounds, in spite of a variation in the three-band spectroscopic parameters that are used to calculate them. This holds for the ratio \tilde{U}/\tilde{t} as well.

$\tilde{U}/\tilde{t} \sim 10$ in all cases, pointing to the effective one-band model being strongly correlated.

As to the spectroscopic values of the three-band parameters, it is generally believed that Δ and t_{pd} measurements are less reliable than those of U_d and U_p . Our estimation procedure Optimization-2 attempts to offer a reasonable description of the spectroscopic and neutron-scattering data by reducing the spread in the values of Δ and t_{pd} across the family of cuprates.

In conclusion, we have performed a perturbative and exact diagonalization study of a model of a Cu_2O cluster that connects electronic parameters obtained from spectroscopy and the three-band model with values of J

obtained from scattering, band dispersion measurements and the effective one-band Hubbard model.

V. ACKNOWLEDGMENTS

AF thanks JSPS KAKENHI (Grant Numbers JP19K03741 and JP22K03535) and the ‘‘Program for Promoting Researches on the Supercomputer Fugaku’’ (Basic Science for Emergence and Functionality in Quantum Matter, JPMXP1020200104) from MEXT. AC thanks the National Science and Technology Council (NSTC) of the Republic of China, Taiwan for financially supporting this research under Contract No. MOST 111-2112-M-213-031.

-
- ¹ B. Keimer, S. A. Kivelson, M. R. Norman, S. Uchida and J. Zaanen, *Nature* 518, 179 (2015).
 - ² J. G. Bednorz and K. A. Mueller, *Z. fur Physik B* 64, 189(1986).
 - ³ P. W. Anderson, in *Frontiers and Borderlines in Many-Particle Physics*, edited by J. R. Schrieffer and R. A. Broglia (NorthHolland, Amsterdam, 1988).
 - ⁴ F. C. Zhang and T. M. Rice, *Phys. Rev. B* 37, 3759 (1988).
 - ⁵ G. Baskaran, Z. Zou, P.W. Anderson, *Solid State Comm.*, 63, 973 (1987).
 - ⁶ C. M. Varma, S. Schmitt-Rink, and E. Abrahams, *Solid State Commun.* 62, 681 (1987).
 - ⁷ V. J. Emery, *Phys. Rev. Lett.* 58, 2794 (1987).
 - ⁸ J. Spalek and A. M. Oles, *Physica B* 86-88, 375 (1977).
 - ⁹ H. J. Schulz, *Superconductivity and Antiferromagnetism in the Two-Dimensional Hubbard Model: Scaling Theory* *Europhysics Letters*, EPL 4, 609 (1987).
 - ¹⁰ C. M. Varma, P. B. Littlewood, S. Schmitt-Rink, E. Abrahams, and A. E. Ruckenstein, *Phenomenology of the normal state of Cu-O high-temperature superconductors*, *Phys. Rev. Lett.* 63, 1996 (1989).
 - ¹¹ Daniel F. Agterberg, J. C. Seamus Davis, Stephen D. Edkins, Eduardo Fradkin, Dale J. Van Harlingen, Steven A. Kivelson, Patrick A. Lee, Leo Radzihovsky, John M. Tranquada, Yuxuan Wang, *The Physics of Pair Density Waves*, *Annual Review of Condensed Matter Physics* 11, 231 (2020).
 - ¹² A.R. Bishop, R. M. Martin, K.A. Muller, and Z. Tesanovic, *Z. Phys. B* 76, 413 (1989).
 - ¹³ J. Rossat-Mignod, L. P. Regnault, C. Vettier, P. Bourges, P. Burllet, J. Bossy, J. Y. Henry, and G. Lapertot, *Physica C* 185-189, 86 (1991).
 - ¹⁴ M. Eschrig, *Adv. Phys.* 55, 47 (2006).
 - ¹⁵ M. Le Tacon, G. Ghiringhelli, J. Chaloupka, M. Moretti Sala, V. Hinkov, M. W. Haverkort, M. Minola, M. Bakr, K. J. Zhou, S. Blanco-Canosa, C. Monney, Y. T. Song, G. L. Sun, C. T. Lin, G. M. De Luca, M. Salluzzo, G. Khaliullin, T. Schmitt, L. Braicovich, and B. Keimer, *Nat. Phys.* 7, 725 (2011).
 - ¹⁶ J. M. Tranquada, B. J. Sternlieb, J. D. Axe, Y. Nakamura and S. Uchida, *Nature* 375, 561 (1995).
 - ¹⁷ T. Wu, H. Mayaffre, S. Kramer, M. Horvatic, C. Berthier, W. N. Hardy, R. Liang, D. A. Bonn and M.-H. Julien, *Nature* 477, 191 (2011).
 - ¹⁸ G. Ghiringhelli, M. Le Tacon, M. Minola, S. Blanco-Canosa, C. Mazzoli, N. B. Brookes, G. M. De Luca, A. Frano, D. G. Hawthorn, F. He, T. Loew, M. Moretti Sala, D. C. Peets, M. Salluzzo, E. Schierle, R. Sutarto, G. A. Sawatzky, E. Weschke, B. Keimer, L. Braicovich, *Science* 337, 821 (2012).
 - ¹⁹ J. Chang, E. Blackburn, A. T. Holmes, N. B. Christensen, J. Larsen, J. Mesot, Ruixing Liang, D. A. Bonn, W. N. Hardy, A. Watenphul, M. v. Zimmermann, E. M. Forgan and S. M. Hayden, *Nature Physics* 8, 871 (2012).
 - ²⁰ M. Le Tacon, A. Bosak, S. M. Souliou, G. Dellea, T. Loew, R. Heid, K-P. Bohnen, G. Ghiringhelli, M. Krisch and B. Keimer, *Nature Physics* 10, 52 (2014).
 - ²¹ W. Tabis, Y. Li, M. Le Tacon, L. Braicovich, A. Kreyssig, M. Minola, G. Dellea, E. Weschke, M. J. Veit, M. Ramazanoglu, A. I. Goldman, T. Schmitt, G. Ghiringhelli, N. Barisic, M. K. Chan, C. J. Dorow, G. Yu, X. Zhao, B. Keimer and M. Greven, *Nat. Commun.* 5:5875 doi: 10.1038/ncomms6875 (2014).
 - ²² S. Gerber, H. Jang, H. Nojiri, S. Matsuzawa, H. Yasumura, D. A. Bonn, R. Liang, W. N. Hardy, Z. Islam, A. Mehta, S. Song, M. Sikorski, D. Stefanescu, Y. Feng, S. A. Kivelson, T. P. Devereaux, Z.-X. Shen, C.-C. Kao, W.-S. Lee, D. Zhu, and J.-S. Lee, *Science* 350, 949 (2015).
 - ²³ M.-H. Julien, P. Carretta, M. Horvatic, C. Berthier, Y. Berthier, P. Segransan, A. Carrington, and D. Colson, *Phys. Rev. Lett.* 76, 4238(1996).
 - ²⁴ W. S. Lee, J. J. Lee, E. A. Nowadnick, S. Gerber, W. Tabis, S. W. Huang, V. N. Strocov, E. M. Motoyama, G. Yu, B. Moritz, H. Y. Huang, R. P. Wang, Y. B. Huang, W. B. Wu, C. T. Chen, D. J. Huang, M. Greven, T. Schmitt, Z. X. Shen and T. P. Devereaux, *Nature Physics* 10, 883 (2014).
 - ²⁵ M. K. Chan, C. J. Dorow, L. Mangin-Thro, Y. Tang, Y. Ge, M. J. Veit, G. Yu, X. Zhao, A. D. Christianson, J. T. Park, Y. Sidis, P. Steffens, D. L. Abernathy, P. Bourges and M. Greven, *Nature Communications* 7, 10819 (2016).
 - ²⁶ M. I. Salkola, V. J. Emery, and S. A. Kivelson, *Phys. Rev.*

- Lett. 77, 155 (1996).
- 27 A. Lanzara, P. V. Bogdanov, X. J. Zhou, S. A. Kellar, D. L. Feng, E. D. Lu, T. Yoshida, H. Eisaki, A. Fujimori, K. Kishio, J.-I. Shimoyama, T. Noda, S. Uchida, Z. Hussain and Z.-X. Shen, *Nature* 412, 510 (2001).
 - 28 J. Zaanen, G. A. Sawatzky and J. W. Allen, *Phys. Rev. Lett.* 55, 418 (1985).
 - 29 C. T. Chen, L. H. Tjeng, J. Kwo, H. L. Kao, P. Rudolf, F. Sette, and R. M. Fleming, *Phys. Rev. Lett.* 68, 2543 (1992).
 - 30 N. B. Brookes, G. Ghiringhelli, O. Tjernberg, L. H. Tjeng, T. Mizokawa, T.W. Li and A. A. Menovsky, *Phys. Rev. Lett.* 87, 237003 (2001).
 - 31 N.B. Brookes, G. Ghiringhelli, A.-M. Charvet, A. Fujimori, T. Kakeshita, H. Eisaki, S. Uchida, and T. Mizokawa, *Phys. Rev. Lett.* 115, 027002 (2015).
 - 32 Daniel I. Khomskii, Section 12.10, *Basic Aspects of the Quantum Theory of Solids*, Cambridge University Press (2010), ISBN-13 978-0-511-78832-1 (eBook).
 - 33 E. Koch, *The Physics of Correlated Insulators, Metals, and Superconductors Modeling and Simulation Vol. 7*, E. Pavarini, E. Koch, R. Scalettar, and R. Martin (eds.), Forschungszentrum Julich, (Julich 2017). ISBN 978-3-95806-224-5.
 - 34 M. Schluter, M. S. Hybertsen, and N. E. Christensen, *Physica C* 153-155, 1217 (1988); M. S. Hybertsen, M. Schluter, and N. E. Christensen, *Phys. Rev. B* 39, 9028 (1989).
 - 35 H. Eskes, G. A. Sawatzky, and L. F. Feiner, *Physica C* 160, 424(1989).
 - 36 A. K. McMahan, J. F. Annett and R. M. Martin, Cuprate parameters from numerical Wannier functions, *Phys. Rev. B* 42, 6268 (1990).
 - 37 P. Werner, R. Sakuma, F. Nilsson, and F. Aryasetiawan, *Phys. Rev. B* 91, 125142 (2015).
 - 38 M. Hirayama, Y. Yamaji, T. Misawa and M. Imada, *Phys. Rev. B* 98, 134501 (2018).
 - 39 A. Fujimori, E. Takayama-Muromachi, Y. Uchida, and B. Okai, *Phys. Rev. B* 35, 8814(R) (1987).
 - 40 Z.-X. Shen, J. W. Allen, J. J. Yeh, J. -S. Kang, W. Ellis, W. Spicer, I. Lindau, M. B. Maple, Y. D. Dalichaouch, M. S. Torikachvili, J. Z. Sun, and T. H. Geballe, *Phys. Rev. B* 36, 8414 (1987).
 - 41 F. Mila, *Phys. Rev. B* 38, 11358 (1988).
 - 42 H. Eskes, L. H. Tjeng, and G. A. Sawatzky, *Phys. Rev. B* 41, 288 (1990).
 - 43 M.E. Simon, M. Balina and A.A. Aligia, *Physica C*, 206, 297 (1993).
 - 44 M.E. Simon and A.A. Aligia, *Phys. Rev. B* 48, 7471 (1993).
 - 45 M. Guerrero, J. E. Gubernatis, and S. Zhang, *Phys. Rev. B* 57, 11980 (1998)
 - 46 D. Senechal, D. Perez, and M. Pioro-Ladriere, 84, 522 (2000).
 - 47 A. Go and A. J. Millis, *Phys. Rev. Lett.* 114, 016402 (2015).
 - 48 E. W. Huang, C. B. Mendl, S. Liu, S. Johnston, H.-C. Jiang, B. Moritz, and T. P. Devereaux, *Science* 358 1161 (2017).
 - 49 E. Vitali, H. Shi, A. Chiciak, and S. Zhang, *Phys. Rev. B* 99, 165116 (2019).
 - 50 M Cini, *Solid State Communications* 20, 605 (1976); 24, 681-684 (1977); *Phys. Rev. B* 17, 2788 (1978).
 - 51 G. A. Sawatzky, *Phys. Rev. Lett.* 39, 504 (1977).
 - 52 A. Balzarotti, M. De Crescenzi, N. Motta, F. Patella, and A. Sgarlata, *Phys. Rev. B* 38, 6461 (1988).
 - 53 D. van der Marel, J. van Elp, G. A. Sawatzky, and D. Heitmann, *Phys. Rev. B* 37, 5136 (1988).
 - 54 L. H. Tjeng, C. T. Chen, and S-W. Cheong, *Phys. Rev. B* 45, 8205 (1992).
 - 55 R. Bar-Deroma, J. Felsteiner, R. Brener, J. Ashkenazi and D. van der Marel *Phys. Rev. B* 45, 2361 (1992).
 - 56 J. Zaanen and G. A. Sawatzky, *Can. J. Phys.* 65, 1262 (1987).
 - 57 Mi Jiang, M. Berciu, and G. A. Sawatzky, *Phys. Rev. Lett.* 124, 207004 (2020).
 - 58 Y. F. Kung, C.-C. Chen, Y. Wang, E. W. Huang, E. A. Nowadnick, B. Moritz, R. T. Scalettar, S. Johnston, and T. P. Devereaux, Characterizing the three-orbital Hubbard model with determinant quantum Monte Carlo. *Phys. Rev. B* 93, 155166 (2016).
 - 59 R. Coldea, S. M. Hayden, G. Aeppli, T. G. Perring, C. D. Frost, T. E. Mason, S.-W. Cheong, and Z. Fisk, *Phys. Rev. Lett.* 86, 5377(2001).
 - 60 P. W. Leung, B. O. Wells, and R. J. Gooding, *Phys. Rev. B* 56. 6320 (1997).
 - 61 C. Kim, P. J. White, Z.-X. Shen, T. Tohyama, Y. Shibata, S. Maekawa, B. O. Wells, Y. J. Kim, R. J. Birgeneau, and M. A. Kastner, *Phys. Rev. Lett.* 80, 4245 (1998).
 - 62 R. Neudert, S.-L. Drechsler, J. Malek, H. Rosner, M. Kielwein, Z. Hu, M. Knupfer, M. S. Golden, J. Fink, N. Nucker, M. Merz, S. Schuppler, N. Motoyama, H. Eisaki, S. Uchida, M. Domke and G. Kaindl, Four-band extended Hubbard Hamiltonian for the one-dimensional cuprate Sr_2CuO_3 : Distribution of oxygen holes and its relation to strong intersite Coulomb interaction, *Phys. Rev. B* 62, 10752 (2000).
 - 63 K. Okada and A. Kotani, *J. Phys. Soc. Jpn.* 66, 341 (1997).
 - 64 T. Boske, O. Knauff, R. Neudert, M. Kielwein, M. Knupfer, M. S. Golden, J. Fink, H. Eisaki, S. Uchida K. Okada, A. Kotani, *Phys. Rev. B* 56, 3438 (1997).
 - 65 M. A. van Veenendaal, H. Eskes, and G. A. Sawatzky, *Phys. Rev. B* 47, 11462 (1993).
 - 66 M. A. van Veenendaal and G. A. Sawatzky, Nonlocal Screening Effects in 2p X-Ray Photoemission Spectroscopy Core-Level Line Shapes of Transition Metal Compounds, *Phys. Rev. Lett.* 70, 2459 (1993).
 - 67 K. Okada, *J. Phys. Soc. Jpn.*, 78, 034725 (2009).
 - 68 N. Nucker, E. Pellegrin, P. Schweiss, J. Fink, S. L. Molodtsov, C. T. Simmons, G. Kaindl, W. Frentrup, A. Erb and G. Muller-Vogt, *Phys. Rev. B* 51, 8529(1995).
 - 69 Andrzej M. Oles and Wojciech Grzelka, Electronic structure and correlations of CuO_3 chains in $\text{YBa}_2\text{Cu}_3\text{O}_7$, *Phys. Rev. B* 44, 9531(1991).
 - 70 M. A. van Veenendaal, G. A. Sawatzky, and W. A. Groen, Electronic structure of $\text{Bi}_2\text{Sr}_2\text{Ca}_{1-x}\text{Y}_x\text{CuO}_{8+\delta}$. Cu 2p x-ray-photoelectron spectra and occupied and unoccupied low-energy states, *Phys. Rev B* 49, 1407 (1994).
 - 71 A. C. Walters, T. G. Perring, J.-S. Caux, A. T. Savici, G. D. Gu, C.-C. Lee, W. Ku and I. A. Zaliznyak, Effect of covalent bonding on magnetism and the missing neutron intensity in copper oxide compounds, *Nat. Phys.* 5, 867 (2009).
 - 72 P. Bourges, H. Casalta, A. S. Ivanov, and D. Petitgrand, *Phys. Rev. Lett.* 79, 4906 (1997).
 - 73 S.M. Hayden, G. Aeppli, T.G. Perring, H.A. Mook, and F. Dogan, *Phys. Rev. B* 54, R6905 (1996).
 - 74 M. P. M. Dean et al. High-energy magnetic excitations in the cuprate superconductor $\text{Bi}_2\text{Sr}_2\text{CaCu}_2\text{O}_{8+\delta}$: Towards a unified description of its electronic and magnetic degrees

- of freedom. Phys. Rev. Lett. 110, 147001 (2013).
- ⁷⁵ Peng, Y. Y. et al. Magnetic excitations and phonons simultaneously studied by resonant inelastic x-ray scattering in optimally doped $\text{Bi}_{1.5}\text{Pb}_{0.55}\text{Sr}_{1.6}\text{La}_{0.4}\text{CuO}_{6+\delta}$, Phys. Rev. B 92, 064517 (2015).
- ⁷⁶ Lichen Wang, Guan hong He, Zichen Yang, Mirian Garcia-Fernandez, Kejin Zhou, Matteo Minola, Matthieu Le Tacon, Bernhard Keimer, Abhishek Nag, Yingying Peng and Yuan Li, Paramagnons and high-temperature superconductivity in a model family of cuprates, Nat. Comm. 13:3163(2022) <https://doi.org/10.1038/s41467-022-30918-z>.
- ⁷⁷ Y. Y. Peng, E. W. Huang, R. Fumagalli, M. Minola, Y. Wang, X. Sun, Y. Ding, K. Kummer, X. J. Zhou, N. B. Brookes, B. Moritz, L. Braicovich, T. P. Devereaux, and G. Ghiringhelli, Dispersion, damping, and intensity of spin excitations in the monolayer $(\text{Bi,Pb})_2(\text{Sr,L a})_2\text{CuO}_{6+\delta}$ cuprate superconductor family, Phys. Rev. B 98, 144507 (2018).
- ⁷⁸ S. Johnston, F. Vernay and T. P. Devereaux, Impact of an oxygen dopant in $\text{Bi}_2\text{Sr}_2\text{CaCu}_2\text{O}_{8+\delta}$, Europhys. Lett. 86, 37007 (2009).
- ⁷⁹ H. Jacobsen, S. M. Gaw, A. J. Princep, E. Hamilton, S. Toth, R. A. Ewings, M. Enderle, E. M. Hetroy Wheeler, D. Prabhakaran, and A. T. Boothroyd, Spin dynamics and exchange interactions in CuO measured by neutron scattering, Phys. Rev. B 97, 144401 (2018).
- ⁸⁰ E. Zurek, O. Jepsen, and O. K. Andersen, ChemPhysChem 6, 1934 (2005).
- ⁸¹ Lipscombe, O. J., Hayden, S. M., Vignolle, B., McMorrow, D. F. and Perring, T. G. Persistence of high-frequency spin fluctuations in overdoped superconducting $\text{La}_{2-x}\text{Sr}_x\text{CuO}_4$ ($x = 0.22$). Phys. Rev. Lett. 99, 067002 (2007).
- ⁸² L. Braicovich, et al. Magnetic excitations and phase separation in the underdoped $\text{La}_{2-x}\text{Sr}_x\text{CuO}_4$ superconductor measured by resonant inelastic x-ray scattering. Phys. Rev. Lett. 104, 077002 (2010).
- ⁸³ M. P. M. Dean et al. Spin excitations in a single La_2CuO_4 layer. Nature Mater. 11, 850?584 (2012).
- ⁸⁴ G. Levy, M. Yaari, T. Z. Regier, and A. Keren, Experimental determination of superexchange energy from two-hole spectra, Cond-mat arXiv:2107.09181v1 (2021).